Icarus 224 (2013) 1–13

Contents lists available at SciVerse ScienceDirect

Icarus

journal homepage: www.elsevier.com/locate/icarus

Near Earth Asteroids with measurable Yarkovsky effect

D. Farnocchia [a,b,*], S.R. Chesley [a], D. Vokrouhlický [c], A. Milani [d], F. Spoto [d], W.F. Bottke [e]

[a] Jet Propulsion Laboratory/Caltech, 4800 Oak Grove Drive, Pasadena, 91109 CA, USA
[b] SpaceDyS, Via Mario Giuntini 63, 56023 Cascina, Pisa, Italy
[c] Institute of Astronomy, Charles University, V Holešovičkách 2, CZ-18000 Prague 8, Czech Republic
[d] Department of Mathematics, University of Pisa, Largo Pontecorvo 5, 56127 Pisa, Italy
[e] Department of Space Studies, Southwest Research Institute, 1050 Walnut St., Boulder, 80302 CO, USA

ARTICLE INFO

Article history:
Received 19 December 2012
Revised 1 February 2013
Accepted 7 February 2013
Available online 16 February 2013

Keywords:
Asteroids, Dynamics
Celestial mechanics
Near-Earth objects
Orbit determination

ABSTRACT

We seek evidence of the Yarkovsky effect among Near Earth Asteroids (NEAs) by measuring the Yarkovsky-related orbital drift from the orbital fit. To prevent the occurrence of unreliable detections we employ a high precision dynamical model, including the Newtonian attraction of 16 massive asteroids and the planetary relativistic terms, and a suitable astrometric data treatment. We find 21 NEAs whose orbital fits show a measurable orbital drift with a signal to noise ratio (SNR) greater than 3. The best determination is for asteroid (101955) 1999 RQ_{36}, with an SNR $\sim$ 200. In some cases it is possible to constrain physical quantities otherwise unknown. Furthermore, the distribution of the detected orbital drifts shows an excess of retrograde rotators that can be connected to the delivery mechanism from the most important NEA feeding resonances and allows us to infer the obliquity distribution of NEAs. We discuss the implications of the Yarkovsky effect for impact predictions. In particular, for asteroid (29075) 1950 DA our results favor a retrograde rotation, which may have implications for the 2880 impact threat.

1. Introduction

It is well known that nongravitational forces should be considered as important as collisions and gravitational perturbations for the overall understanding of asteroid evolution (Bottke et al., 2006). The most important nongravitational perturbation is the Yarkovsky effect, which is due to radiative recoil of anisotropic thermal emission and causes asteroids to undergo a secular semimajor axis drift da/dt. Typical values of da/dt for sub-kilometer NEAs are 10^{-4}–10^{-3} au/Myr (Vokrouhlický et al., 2000).

The Yarkovsky acceleration depends on several physical quantities such as spin state, size, mass, shape, and thermal properties (Vokrouhlický, 1999). Furthermore, Rozitis and Green (2012) show that surface roughness also plays an important role by enhancing the Yarkovsky related semimajor axis drift by as much as tens of per cent. Though no complete physical characterization is typically available to compute the Yarkovsky acceleration based on a thermophysical model, the orbital drift may be detectable from an astrometric dataset. As a matter of fact, purely gravitational dynamics could result in an unsatisfactory orbital fit to the observational data. This is especially true when extremely accurate observations are available, e.g., radar observations, or when the observational dataset spans a long time interval thus allowing the orbital drift to accumulate and become detectable.

Until recently, the Yarkovsky effect has been measured directly only in three cases, (6489) Golevka (Chesley et al., 2003), (152563) 1992 BF (Vokrouhlický et al., 2008), and recently for (101955) 1999 RQ_{36} (Chesley et al., 2012). For both Golevka and 1999 RQ_{36} the Yarkovsky perturbation must be included to fit accurate radar observations spanning three apparitions. For 1992 BF the Yarkovsky effect is needed to link four precovery observations of 1953. Furthermore, in the case of 1999 RQ_{36} the available physical characterization, along with the estimate of the Yarkovsky effect, allows the estimate of the asteroid's bulk density.

Nugent et al. (2012b) find 54 detections of semimajor axis drift by performing a search for semimajor axis drift among NEAs similar to the one presented in this paper. However, there are differences in the observational data treatment, in the modeling, and in the selection filters. A description of the differences and a comparison of the results is provided in Section 3.2. Nugent et al. (2012a) use WISE-derived geometric albedos and diameters to predict orbital drifts for 540 NEAs. Even if none of these objects has an observational record that allows one to measure the predicted orbital drift, the authors list upcoming observing opportunities that may reveal the Yarkovsky signal.

The Yarkovsky effect plays an important role for orbital predictions such as those concerning Earth impacts. In particular, when an asteroid has an exceptionally well constrained orbit, the Yarkovsky effect may become the principal source of uncertainty. Milani et al. (2009) show how the size of the semimajor axis drift along with its uncertainty modifies impact predictions for the next century for 1999 RQ_{36}. The cumulative impact probability is

* Corresponding author at: Jet Propulsion Laboratory/Caltech, 4800 Oak Grove Drive, Pasadena, 91109 CA, USA.
E-mail address: Davide.Farnocchia@jpl.nasa.gov (D. Farnocchia).

0019-1035/$ - see front matter © 2013 Elsevier Inc. All rights reserved.
http://dx.doi.org/10.1016/j.icarus.2013.02.004

approximately 10^{-3}, while a Yarkovsky-free propagation would rule out any impact event. Chesley et al. (2012) improve the da/dt estimate by means of September 2011 Arecibo radar measurements and find a cumulative impact probability approximately 4×10^{-4}. Another remarkable case is (99942) Apophis. Though only a marginal da/dt estimate is available, Giorgini et al. (2008) and Chesley et al. (2009) prove that the occurrence of an impact in 2036 is decisively driven by the magnitude of the Yarkovsky effect. In the longer term, Giorgini et al. (2002) show that an impact between asteroid (29075) 1950 DA and the Earth in 2880 depends on the accelerations arising from thermal re-radiation of solar energy absorbed by the asteroid.

2. Methodology

2.1. Yarkovsky modeling and determination

The Yarkovsky effect depends on typically unknown physical quantities. As the primary manifestation is a semimajor axis drift, we seek a formulation depending on a single parameter to be determined simultaneously with the orbital elements from the observational dataset. To bypass the need of physical characterization we used a comet-like model (Marsden et al., 1973) for transverse acceleration $a_t = A_2\, g(r)$, where g is a suitable function of the heliocentric distance r and A_2 is an unknown parameter.

For a given A_2 we estimate semimajor axis drift by means of Gauss' perturbative equations:

$$\dot{a} = \frac{2a\sqrt{1-e^2}}{nr} A_2 g(r) \tag{1}$$

where a is the semimajor axis, e is the eccentricity and n is the mean motion. By averaging we obtain

$$\bar{\dot{a}} = \frac{a\sqrt{1-e^2}A_2}{\pi} \int_0^T \frac{g(r)}{r}\, dt = \frac{A_2}{\pi n a} \int_0^{2\pi} r g(r)\, df \tag{2}$$

where T is the orbital period and f is the true anomaly. Let us now assume $g(r) = (r_0/r)^d$, where r_0 is a normalizing parameter, e.g., we use $r_0 = 1$ au. In this case the semimajor axis drift is

$$\bar{\dot{a}} = \frac{A_2(1-e^2)}{\pi n} \left(\frac{r_0}{p}\right)^d \int_0^{2\pi} (1 + e\cos f)^{d-1}\, df \tag{3}$$

By Taylor expansion, we have

$$\int_0^{2\pi} (1 + e\cos f)^{d-1}\, df = \sum_{k=0}^{\infty} \binom{d-1}{k} e^k \int_0^{2\pi} \cos^k f\, df \tag{4}$$

The odd powers of the cosine average out, so we obtain

$$\bar{\dot{a}} = \frac{2A_2(1-e^2)}{n} \left(\frac{r_0}{p}\right)^d J(e,d) \tag{5}$$

where

$$J(e,d) = \sum_{k=0}^{\infty} \alpha_k e^{2k}, \quad \alpha_k = \binom{d-1}{2k} \binom{2k}{k} \frac{1}{2^{2k}} \tag{6}$$

The ratio

$$\frac{\alpha_{k+1}}{\alpha_k} = \left(1 - \frac{d+1}{2k+2}\right)\left(1 - \frac{d}{2k+2}\right) \tag{7}$$

is smaller than 1 for $d > 0$ and k large enough. Therefore, α_k are bounded and $J(e,d)$ is convergent for any $e < 1$. Eq. (7) can be used to recursively compute α_k starting from $\alpha_0 = 1$. For integer d the series J is a finite sum that can be computed analytically, e.g., $J(e,2) = 1$ and $J(e,3) = 1 + 0.5e^2$.

For a fixed d we have a transverse acceleration $a_t = A_2(r_0/r)^d$. To determine A_2 we used a 7-dimensional differential corrector: starting from the observational dataset we simultaneously determine a best-fitting solution for both the orbital elements and A_2 along with an associated covariance matrix C describing the uncertainty of the nominal solution. The marginal uncertainty of A_2 is obtained from C: $\sigma_{A_2} = \sqrt{c_{77}}$, where c_{ij} is the generic element of C. This uncertainty is then mapped to the uncertainty of the semimajor axis drift by means of Eq. (5).

The proper value of d is not easily determined. From Vokrouhlický (1998), we have

$$a_t \simeq \frac{4(1-A)}{9} \Phi(r) f(\Theta) \cos\gamma, \quad f(\Theta) = \frac{0.5\Theta}{1 + \Theta + 0.5\Theta^2} \tag{8}$$

for the Yarkovsky diurnal component (which is typically dominant), where A is the Bond albedo, Θ is the thermal parameter, γ is the obliquity, and $\Phi(r)$ is the standard radiation force factor, which is inversely proportional to the bulk density ρ, the diameter D, and r^2. The thermal parameter Θ is related to the thermal inertia Γ by means of the following equation

$$\Theta = \frac{\Gamma}{\varepsilon\sigma T_*^3} \sqrt{\frac{2\pi}{P}} \tag{9}$$

where ε is the emissivity, σ is the Boltzmann's constant, T_* is the subsolar temperature, and P is the rotation period. In this paper we use $d = 2$ to match the level of absorbed solar radiation. Then, from Eq. (8) we have that

$$A_2 \simeq \frac{4(1-A)}{9} \Phi(1\text{ au}) f(\Theta) \cos\gamma \tag{10}$$

However, as $T_* \propto r^{-0.5}$ we have that $\Theta \propto r^{1.5}$, therefore the best value of d depends on the object's thermal properties:

- for $\Theta \gg 1$ we obtain $f \propto r^{-1.5}$, which gives $d = 3.5$;
- for $\Theta \ll 1$ we obtain $f \propto r^{1.5}$, which gives $d = 0.5$.

These are limit cases, the true d is always going to be between them. As a matter of fact, it turns out that most NEAs, whose rotation period is not excessively large and whose surface thermal inertia is not excessively small or large, have typically values of Θ near unity or only slightly larger, and we can thus expect d values in the range 2–3. As an example, Chesley et al. (2012) show that for 1999 RQ_{36} the best match to the Yarkovsky perturbation computed by using a linear heat diffusion model is $d = 2.75$.

What matters to us is that da/dt does not critically depend on the chosen value of d. As an example for asteroid 1999 RQ_{36} we have that $da/dt = (-18.99 \pm 0.10) \times 10^{-4}$ au/Myr for $d = 2$ and $da/dt = (-19.02 \pm 0.10) \times 10^{-4}$ au/Myr for $d = 3$. Another example is Golevka, for which we obtain $da/dt = (-6.62 \pm 0.64) \times 10^{-4}$ au/Myr for $d = 2$ and $da/dt = (-6.87 \pm 0.66) \times 10^{-4}$ au/Myr for $d = 3$. In both cases the difference in da/dt due to the different values assumed for d is well within one standard deviation.

2.2. Dynamical model

To consistently detect the Yarkovsky effect we need to account for the other accelerations down to the same order of magnitude. For a sub-kilometer NEA, typical values of a_t range from 10^{-15} to 10^{-13} au/d^2.

Our N-body model includes the Newtonian accelerations of the Sun, eight planets, the Moon, and Pluto that are based on JPL's DE405 planetary ephemerides (Standish, 2000). Furthermore, we added the contribution of 16 massive asteroids, as listed in Table 1.

We used a relativistic force model including the contribution of the Sun, the planets, and the Moon. Namely, we used the Einstein–Infeld–Hoffman (EIH) approximation as described in Moyer (2003) or Will (1993). As already noted in Chesley et al. (2012),

Table 1
Gravitational parameters of perturbing asteroids. The masses of Ceres, Pallas, and Vesta are from Standish and Hellings (1989), the ones of Euphrosyne and Herculina are from the Institute of Applied Astronomy of RAS, St. Petersburg, Russia (http://www.ipa.nw.ru/PAGE/DEPFUND/LSBSS/engmasses.htm), the mass of Juno is from Konopliv et al. (2011), all the others are from Baer et al. (2011).

Asteroid	Gm (km^3/s^2)
(1) Ceres	63.200
(2) Pallas	14.300
(4) Vesta	17.800
(10) Hygea	6.0250
(29) Amphitrite	1.3271
(511) Davida	3.9548
(65) Cybele	1.0086
(9) Metis	1.3669
(15) Eunomia	2.2295
(31) Euphrosyne	1.1280
(52) Europa	1.2952
(704) Interamnia	4.7510
(16) Psyche	1.7120
(3) Juno	1.9774
(532) Herculina	1.5262
(87) Sylvia	1.3138

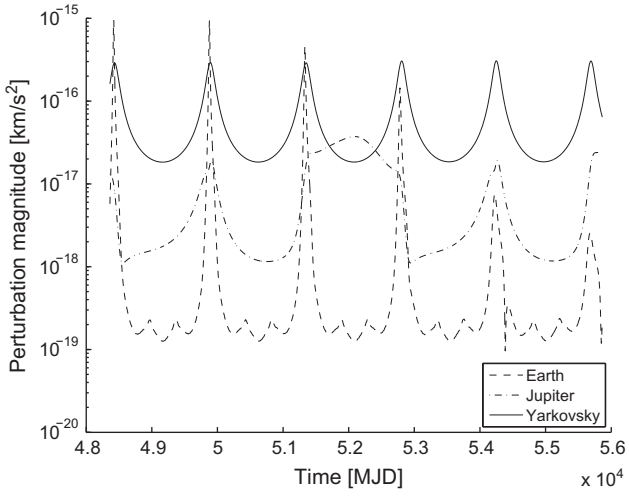

Fig. 1. Relativistic accelerations of the Earth and Jupiter as they formally appear in the EIH equations of motion compared to the transverse Yarkovsky acceleration acting on Golevka.

the relativistic term of the Earth should not be neglected because of significant short range effects during Earth approaches that NEAs may experience. For asteroids with a large perihelion distance such as Golevka also Jupiter's term could be relevant. Fig. 1 compares the relativistic accelerations of the Earth and Jupiter as they formally appear in the EIH equations of motion to the transverse Yarkovsky acceleration acting on Golevka.

2.3. Observational error model

The successful detection of the Yarkovsky effect as a result of the orbital fit strongly depends on the quality of the observations involved. In particular, the availability of radar data is often decisive due to the superior relative accuracy of radar data with respect to optical ones. Moreover, radar measurements are orthogonal to optical observations: range and range rate vs. angular position in the sky.

Since the Yarkovsky effect acts as a secular drift on semimajor axis we have a quadratic effect in mean anomaly: the longer the time span the stronger the signal. However, the presence of biases in historical data and unrealistic weighting of observations may lead to inaccurate results. To deal with this problem we applied the debiasing and weighting scheme described in Chesley et al. (2010). This scheme is a valid error model for CCD observations, while for pre-CCD data the lack of star catalog information and the very uneven quality of the observations represents a critical problem. In these cases the occurrence of unrealistic nominal values for Yarkovsky model parameters presumably point to bad astrometric treatments and have to be rejected.

To prevent outliers from spoiling orbital fits, we applied the outlier rejection procedure as described in Carpino et al. (2003).

Besides the astrometric treatment described above, in the following cases we applied an ad hoc observation weighting:

- 1999 RQ_{36}: as already explained by Chesley et al. (2012), in some cases there are batches containing an excess of observations from a single observatory in a single night. In particular there are four nights, each with about 30 observations from observatory La Palma. To reduce the effect of these batches to a preferred contribution of 5 observations per night, we relaxed the weight by a factor $\sqrt{N/5}$, where N is the number of observations contained in the batch.
- 1992 BF: as the precovery observations of 1953 have been carefully remeasured in Vokrouhlický et al. (2008), these observations were given a weight at 0.5″ in right ascension and 1″ in declination.
- Apollo: the large dataset available for Apollo contains observations going back to 1930. Many pre-CCD era observation batches show unusually high residuals, especially during close Earth approaches. To lower the effect of non-CCD observation, we used weights at 10″ for observations from 1930 to 1950 and 3″ from 1950 to 1990. By using weights at 10″ we made sure we included all non-CCD observations, thus reducing the average error and avoiding to fit a possibly inaccurate subset only.
- 1989 ML: the discovery apparition contains observations from Palomar Mountain showing large residuals whether or not the Yarkovsky perturbation is included in the model. Even if this apparition increases the observed arc by only 3 years we felt it safer to weight the corresponding observations at 3″.

2.4. Treatment of precovery observations

There are a few cases where the Yarkovsky signal is mainly contained in few isolated precovery observations. This is the case of the already mentioned asteroid 1992 BF, which has four isolated observations in 1953 from Palomar Mountain DSS. Other cases are

- 1999 FK_{21}, which has six isolated observations in 1971 from Palomar Mountain.
- 2001 MQ_3, which has four isolated observations in 1951 from Palomar Mountain DSS.
- 1989 UQ, which has three isolated observations in 1954 from Palomar Mountain.
- 1991 VE, which has four isolated observations in 1954 from Palomar Mountain DSS.

For all these cases it would be desirable to remeasure the precovery observations as was done for 1992 BF in Vokrouhlický et al. (2008), where precovery observations were corrected by an amount of up to 3.1″. For this reason we conservatively gave weights at 3″ to the precovery observations of the four asteroids above.

Besides the conservative weighting, we ruled out clock error as a possible cause of the Yarkovsky signal. Fig. 2 shows the scenario for the four mentioned asteroids during the precovery apparition. We can see that it is not possible to match the observations by

translating the non-Yarkovsky uncertainty ellipse on the along track direction. The Yarkovsky solution produces a shift in the weak direction that give a better match to the observations, in particular when we take the average of the observed positions.

2.5. Filtering spurious results

To assess the reliability of the Yarkovsky detections we computed an expected value for A_2 starting from the 1999 RQ_{36} case, which is the strongest and most reliable detection, by scaling according to (10)

$$(A_2)_{exp} = (A_2)_{RQ36}\frac{D_{RQ36}}{D} \tag{11}$$

For diameter D we used either the known value when available or an assumed value computed from the absolute magnitude H according to the following relationship (Pravec and Harris, 2007):

$$D = 1329\ \text{km} \times \frac{10^{-0.2H}}{\sqrt{p_V}} \tag{12}$$

where p_V is the albedo, assumed to be 0.154 if unknown, in agreement with Chesley et al. (2002).

Some physical properties of 1999 RQ_{36} maximize A_2 (Chesley et al., 2012). In particular γ is nearly 180°, A is 0.01, and ρ is low (0.96 g/cm^3). On the other hand $\Theta = 4.33$ for which $f(\Theta) \simeq 0.15$ while the maximum is $\simeq$0.21. For these reasons we selected those Yarkovsky detections for which $\mathscr{S} = |A_2/(A_2)_{exp}|$ was smaller than 1.5. The selected threshold allows some tolerance as we are scaling only by D without accounting for other quantities such as bulk density, thermal properties, obliquity, spin rate, and surface roughness.

A high signal to noise ratio SNR $= |A_2|/\sigma_{A_2}$ threshold is likely to produce robust detections with respect to the astrometric data treatment. With lower SNR the sensitivity to the observation error model increases and detections become less reliable. We decided that 3 was a sensible choice for minimum SNR, even if we analyze detections with smaller SNR in Section 3.3.

3. Results

We applied our 7-dimensional differential corrector to determine the parameter A_2 and the corresponding da/dt for all known NEAs. After applying the filters discussed in Section 2.5 we obtain 21 Yarkovsky detections that we consider reliable (Table 2). The reported uncertainties are marginal, i.e., they fully take into account the correlation between A_2 (and thus da/dt) and the orbital elements.

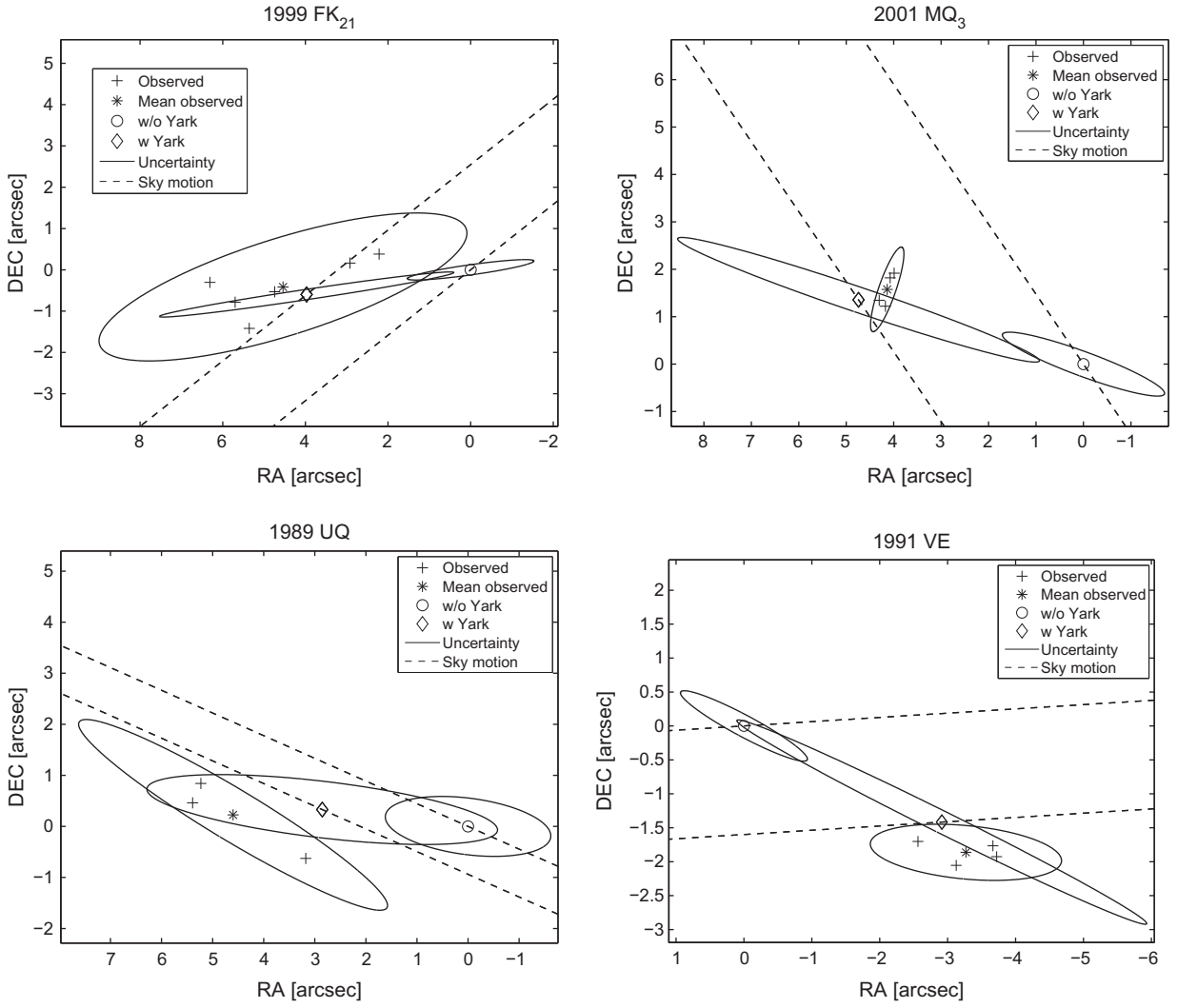

Fig. 2. Observed position, average observed position, and predicted postfit position both with and without the Yarkovsky perturbation in the dynamics. The uncertainty ellipses for the mean observed position and the predicted positions correspond to the 3-σ level. The dashed lines represent the predicted motion in the sky of the asteroid in the precovery apparition. Circles are the predicted positions, crosses are the measured positions, stars are the mean of the measured positions, while diamonds are the predicted positions when the Yarkovsky perturbation is included in the dynamics. The origin is arbitrarily set to the non-Yarkovsky prediction.

Table 2
Semimajor axis, eccentricity, absolute magnitude, physical and Yarkovsky parameters, and observational information for selected NEAs. The physical quantities for 1999 RQ_{36} are from Chesley et al. (2012). Golevka's obliquity γ is from Hudson et al. (2000), Apollo's from Ďurech et al. (2008b), Nyx's from Drummond and Wisniewski (1990), Ra-Shalom's from Ďurech et al. (2012), YORP's from Taylor et al. (2007), Geographos' from Ďurech et al. (2008a), and Toro's from Ďurech (personal communication). Diameters D and rotation periods P are from the European Asteroid Research Node (EARN) database (http://earn.dlr.de/nea/). Bond albedo A was computed from geometric albedo p_V and slope parameter G (both from the EARN database when available) by $A = (0.290 + 0.684G)p_V$ (Bowell et al., 1989).

Asteroid	a (au)	e	H	D (km)	P (h)	A	γ	A_2 (10^{-15} au/d^2)	SNR	$\mathscr{S}$	da/dt (10^{-4} au/Myr)	da/dt Nugent et al.	Diff. σ	Observed arc	Radar apparitions
(101955) 1999 RQ_{36}	1.13	0.20	20.6	0.49	4.29	0.01	175°	−45.49 ± 0.23	197.7	1.0	−18.99 ± 0.10	−18.9 ± 0.2	0.4	1999–2012	1999, 2005, 2011
(152563) 1992 BF	0.91	0.27	19.6	0.51	NA	0.02	NA	−24.01 ± 1.21	19.8	0.5	−11.55 ± 0.58	−12.84 ± 1	1.1	1953–2011	NA
(6489) Golevka	2.52	0.60	19.1	0.27	6.03	0.23	137°	−15.88 ± 1.52	10.4	0.2	−6.62 ± 0.64	−5.74 ± 0.7	0.9	1991–2011	1991, 1995, 2003
2009 BD	1.01	0.04	28.2	NA	NA	NA	NA	−1164.01 ± 138.76	8.4	0.4	−493.39 ± 58.81	NA	NA	2009–2011	NA
(1862) Apollo	1.47	0.56	16.0	1.40	3.06	0.12	162°	−3.34 ± 0.52	6.4	0.2	−1.70 ± 0.26	−2.3 ± 0.2	1.8	1930–2012	1980, 2005
(2062) Aten	0.97	0.18	16.9	1.30	40.77	NA	NA	−15.41 ± 2.45	6.3	0.9	−6.29 ± 1.10	−7.5 ± 2.4	0.4	1955–2012	1995, 2012
(3908) Nyx	1.93	0.46	17.3	1.00	4.43	NA	20°	29.95 ± 5.39	5.6	1.3	11.61 ± 2.09	12.9 ± 2.7	0.4	1980–2012	1988, 2004
(10302) 1989 ML	1.27	0.14	19.4	0.25	19	NA	NA	90.48 ± 16.38	5.5	1.0	34.71 ± 6.28	35.3 ± 7.1	0.0	1989–2012	NA
(2100) Ra-Shalom	0.83	0.44	16.1	2.24	19.80	0.05	162°	−10.97 ± 2.25	4.9	1.1	−6.31 ± 1.30	−5.4 ± 1.5	0.5	1975–2012	1981, 1984, 2000, 2003
(85953) 1999 FK_{21}	0.74	0.70	18.0	0.59	NA	NA	NA	−10.62 ± 2.33	4.6	0.3	−10.38 ± 2.28	−10.44 ± 1.5	0.0	1971–2012	NA
1999 MN	0.67	0.67	21.4	NA	5.49	NA	NA	50.79 ± 11.39	4.5	0.4	47.12 ± 10.56	NA	NA	1999–2010	NA
(2340) Hathor	0.84	0.45	19.9	0.30	NA	0.24	NA	−24.71 ± 5.66	4.4	0.3	−14.33 ± 3.28	−14.5 ± 3.5	0.0	1976–2012	NA
(6037) 1988 EG	1.27	0.50	18.7	0.40	2.76	NA	NA	−32.66 ± 8.19	4.0	0.6	−16.39 ± 4.11	−14.2 ± 4.3	0.4	1988–2011	1988
(37655) Illapa	1.48	0.75	17.8	NA	2.66	NA	NA	−13.99 ± 3.65	3.8	0.6	−11.27 ± 2.94	NA	NA	1994–2012	2012
(1685) Toro	1.37	0.44	14.3	3.00	10.20	0.05	144°	−2.83 ± 0.77	3.7	0.4	−1.27 ± 0.34	−1.4 ± 0.7	0.2	1948–2012	1980, 1988 2012
2005 ES_{70}	0.76	0.39	23.6	NA	NA	NA	NA	−97.23 ± 29.27	3.3	0.3	−55.58 ± 16.73	NA	NA	2005–2011	NA
(54509) YORP	1.00	0.23	22.6	0.10	0.20	NA	178°	−74.93 ± 23.68	3.2	0.3	−33.60 ± 10.61	−35.63 ± 10.5	0.1	2000–2005	2001, 2004
(283457) 2001 MQ_3	2.23	0.46	18.9	NA	NA	NA	NA	−44.63 ± 14.33	3.1	1.1	−16.02 ± 5.14	NA	NA	1951–2011	NA
(1620) Geographos	1.25	0.34	15.2	2.47	5.22	NA	153°	−4.25 ± 1.40	3.0	0.5	−1.82 ± 0.60	−2.5 ± 0.6	0.8	1951–2012	1983, 1994
(65679) 1989 UQ	0.91	0.26	19.3	0.73	7.73	NA	NA	−36.66 ± 12.23	3.0	1.2	−17.51 ± 5.84	NA	NA	1954–2011	NA
(162004) 1991 VE	0.89	0.66	18.0	NA	NA	NA	NA	18.30 ± 6.13	3.0	0.7	14.75 ± 4.94	NA	NA	1954–2012	NA

We cross-checked these detections by using two independent software suites: the JPL Comet and Asteroid Orbit Determination Package and OrbFit (http://adams.dm.unipi.it/orbfit/)[1]: in all cases we found agreement at better than the 1-σ level.

3.1. 2009 BD

Despite the short observed arc, asteroid 2009 BD has a quite accurate orbit, e.g., the semimajor axis uncertainty is 5×10^{-8} au. The observational dataset contains some observations rejected as outliers from the Mauna Kea observatory. Micheli et al. (2012) show that including solar radiation pressure allows an improvement in the fit to the observations and the recovery of Mauna Kea observations. Therefore, we also included in the model a radial acceleration $a_r = A_1/r^2$. Along with the tabulated value of A_2, we obtained $A_1 = (62.05 \pm 8.85) \times 10^{-12}$ au/d^2. This results in an area to mass ratio $A/M = (2.72 \pm 0.39) \times 10^{-4}$ m^2/kg, which is consistent at the 1-σ level with the value reported by Micheli et al. (2012), i.e., $(2.97 \pm 0.33) \times 10^{-4}$ m^2/kg.

After including A_1 and A_2 in the orbital solution, the uncertainty in semimajor axis is about 4.3×10^{-8} au, which is significantly smaller than the product between the detected semimajor axis drift and the observed arc time interval, i.e., 1.5×10^{-7} au.

The value of A_2 seems quite large, but it is consistent with the expected size of this object. From the absolute magnitude $H = 28.2$ we obtain an estimated diameter of 8 m and the parameter $\mathscr{S}$ computed accordingly is 0.4.

3.2. Comparison with other published results

The first three objects of Table 2 are the already known cases of Golevka, 1992 BF, and 1999 RQ_{36}. While for 1999 RQ_{36} there is a perfect match between our result and the one in Chesley et al. (2012), for Golevka and 1992 BF the values are different from Chesley et al. (2003) and Vokrouhlický et al. (2008), respectively. However, this can be easily explained by the availability of new astrometry and the fact that the present paper adopted the debiasing and weighting scheme by Chesley et al. (2010), which was not available at the time of the earlier publications.

As already mentioned, Nugent et al. (2012b) performed a search similar to the one presented in this paper and found 54 NEAs with a measurable semimajor axis drift. The main differences are the following:

- They selected only numbered objects, while we included all known NEAs.
- Their observation dataset was slightly different as they used observations until 2012 January 31, while we have data until 2012 October 31. This difference does not really matter for optical data, but it does for radar data, e.g., for Aten and Toro. Moreover, they did not use single apparition radar observations, while we did as we think they represent an important constraint.
- They solved for constant da/dt while we used constant A_2 and then convert to da/dt. These techniques are equivalent when the semimajor axis and eccentricity are constant, but there could be differences as we cannot assume da/dt constant for objects experiencing deep planetary close approaches. However, the error due to close encounter is generally smaller than the da/dt standard deviation.
- They searched for the best-fit da/dt by means of the golden section algorithm, i.e., they computed the RMS of the residuals corresponding to the best fitting orbital elements for fixed values

[1] OrbFit was used in the development version 4.3, currently in beta-testing.

of da/dt, then the minimum is obtained by interpolation. In this paper we used a full 7-dimensional differential corrector. The two methods should be equivalent.
- They used 1 as lower bound for SNR, while we use 3 that gives detections more robust against changes in the observation weighting. Also, they used the "sensitivity" parameter, i.e., a metric to measure the sensitivity of an observational dataset to the presence of a semimajor axis drift. We did not use such a metric as we think that an SNR $\geqslant 3$ is already a good metric in that respect.
- We kept only those objects for which the measured orbital drift can be related to the Yarkovsky perturbation presuming that inconsistencies stem from astrometric errors, while they also considered the possibility of other nongravitational effects such as a loss of mass.

Table 2 contains a comparison between our orbital drifts and the ones reported by Nugent et al. (2012b). 2009 BD, 1999 MN, and 2005 ES_{70} are present only in our list as they are not numbered, while 2001 MQ_3, 1989 UQ, 1991 VE, and Illapa are eliminated by their filters. It is worth pointing out that also 1999 RQ_{36}, Golevka, and YORP have been filtered out by Nugent et al. (2012b) criteria, even though they report the corresponding detections for a comparison with Chesley et al. (2008). This is likely to be due to the lack of radar information in the computation of the sensitivity parameter.

Among the cases that Nugent et al. (2012b) report with SNR > 3 we did not include the following three:

- (1036) Ganymed for which we found $A_2 = (-16.54 \pm 4.35) \times 10^{-15}$ au/d^2, corresponding to $da/dt = (-6.06 \pm 1.59) \times 10^{-4}$ au/Myr. However, the nominal A_2 is 28 times larger than $(A_2)_{exp}$, so we marked this detection as spurious. As Ganymed observations go back to 1924, this unreliable detection might be due to bad quality astrometry.
- (4197) 1982 TA for which we used the radar apparition of 1996, which reduced the SNR below 1. For this object we found $A_2 = (5.61 \pm 14.26) \times 10^{-15}$ au/d^2, corresponding to $da/dt = (3.88 \pm 9.86) \times 10^{-4}$ au/Myr. For comparison Nugent et al. (2012b) report $da/dt = (30.9 \pm 9.2) \times 10^{-4}$ au/Myr.
- (154330) 2002 VX_4 for which we found $A_2 = (102.36 \pm 36.34) \times 10^{-15}$ au/d^2, corresponding to $da/dt = (43.10 \pm 15.25) \times 10^{-4}$ au/Myr. Again, the value of A_2 was $\sim$4 times larger than $(A_2)_{exp}$, so also this detection was marked as spurious.

Besides the differences outlined above, there is an overall agreement for the common cases. As a matter of fact by computing the σ of the difference, i.e., $\sigma^2 = \sigma_1^2 + \sigma_2^2$, there are only two cases that are not consistent at the 1-σ level:

- 1992 BF, for which we applied suitable weights (see Section 2.3) for the remeasured observations (Vokrouhlický et al., 2008) of the 1953 apparition. By using the Chesley et al. (2010) standard weights the uncertainty in da/dt of our detection increases to 0.97×10^{-4} au/Myr, and therefore we are consistent with Nugent et al. (2012b) at the 1-σ level.
- Apollo, for which we applied a suitable manual weighting as described in Section 2.3.

3.3. Lower SNR and small orbital drifts

Table 3 contains detections that we rate as non-spurious on the basis of the $\mathscr{S}$ ratio between expected and measured value, down to SNR = 2 plus the following remarkable cases:

Table 3
Same as Table 2 for less reliable detections. Eros' obliquity is from Yeomans et al. (2000), Nereus' from Brozović et al. (2009), and Betulia's from Drummond and Wisniewski (1990). All the other physical quantities are from the EARN database.

Asteroid	a (au)	e	H	D (km)	P (h)	A	γ	A_2 (10^{-15} au/d^2)	SNR	$\mathscr{S}$	da/dt (10^{-4} au/Myr)	da/dt Nugent et al.	Diff. σ	Observed arc	Radar apparitions
1999 FA	1.07	0.13	20.6	0.30	10.09	NA	NA	−106.94 ± 32.06	3.3	1.4	−44.51 ± 13.35	NA	NA	1978–2008	NA
(433) Eros	1.46	0.22	10.8	23.30	5.27	0.10	89°	−0.72 ± 0.23	3.1	0.7	−0.26 ± 0.09	−0.3 ± 0.2	0.2	1893–2012	1975, 1988
(230111) 2001 BE_{10}	0.82	0.37	19.0	NA	4.20	NA	NA	−38.72 ± 14.00	2.8	0.9	−20.98 ± 7.59	NA	NA	2001–2013	2004
(4660) Nereus	1.49	0.36	18.1	0.34	15.16	NA	11°	28.58 ± 11.72	2.4	0.4	11.43 ± 4.69	10.9 ± 4.8	0.1	1981–2012	2001, 2002
2007 PB_8	0.88	0.45	21.2	NA	NA	NA	NA	−156.01 ± 66.45	2.3	1.4	−88.05 ± 37.50	NA	NA	2002–2012	NA
2004 BG_{41}	2.52	0.61	24.4	NA	NA	NA	NA	−598.99 ± 255.87	2.3	1.2	−256.03 ± 109.37	NA	NA	2004–2011	NA
(4179) Toutatis	2.53	0.63	15.1	2.80	176.00	0.05	NA	−3.32 ± 1.43	2.3	0.4	−1.49 ± 0.63	−5.0 ± 0.6	4.1	1976–2012	1992, 1996, 2000, 2004, 2008
(138911) 2001 AE_2	1.35	0.08	19.0	0.35	NA	NA	NA	−62.23 ± 28.84	2.2	1.0	−22.90 ± 10.61	−22.9 ± 11.2	0.0	1984–2012	NA
(326290) 1998 HE_3	0.88	0.44	21.7	0.10	NA	NA	NA	−70.57 ± 33.01	2.1	0.3	−39.68 ± 18.56	NA	NA	1993–2012	2012
(3361) Orpheus	1.21	0.32	18.9	0.50	3.51	NA	NA	12.07 ± 5.67	2.1	0.3	5.20 ± 2.44	5.7 ± 2.5	0.1	1982–2010	NA
(154590) 2003 MA_3	1.11	0.40	21.7	NA	NA	NA	NA	−95.60 ± 45.11	2.1	0.7	−46.06 ± 21.74	NA	NA	1998–2012	NA
1994 XL_1	0.67	0.53	20.8	NA	NA	NA	NA	−31.22 ± 15.32	2.0	0.3	−22.38 ± 10.98	NA	NA	1994–2011	NA
(1580) Betulia	2.19	0.49	14.3	4.57	6.13	0.03	117°	−4.65 ± 2.31	2.0	0.9	−1.75 ± 0.87	−1.3 ± 0.9	0.4	1950–2012	1976, 1989, 2002
(29075) 1950 DA	1.70	0.51	17.0	1.4	2.12	0.08	NA	−5.00 ± 3.47	1.4	0.3	−2.20 ± 1.52	NA	NA	1950–2012	2001
(250680) 2005 QC_5	0.89	0.36	19.7	NA	NA	NA	NA	26.44 ± 22.01	1.2	0.5	13.70 ± 11.40	NA	NA	1978–2011	NA
(105140) 2000 NL_{10}	0.91	0.82	15.5	1.72	6.93	NA	NA	−11.78 ± 10.49	1.1	0.9	−15.73 ± 14.02	NA	NA	1951–2012	NA

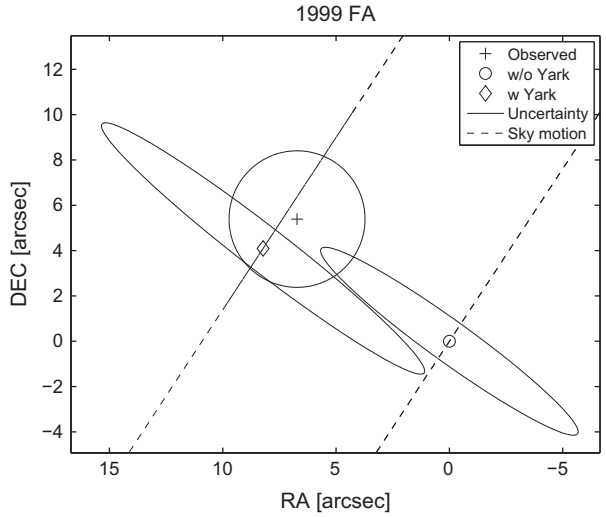

Fig. 3. Same of Fig. 2 for asteroid 1999 FA. The uncertainty ellipses for predicted positions correspond to 3-σ levels, while the uncertainty for the observed position correspond to 3″.

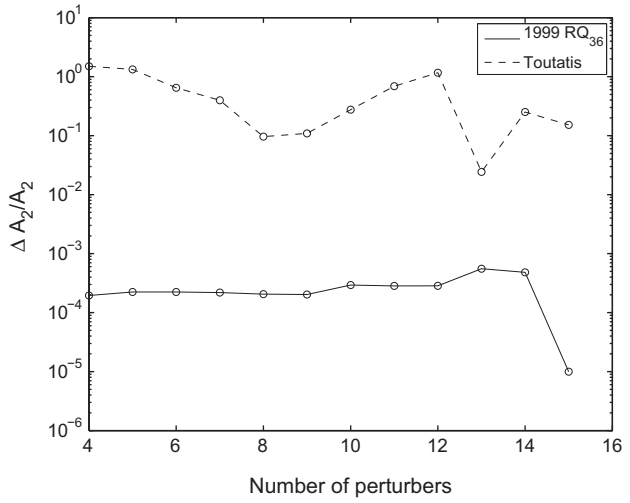

Fig. 4. Relative displacement of A_2 with respect to the nominal value as a function of the number of perturbers for 1999 RQ_{36} and Toutatis.

- 1999 FA, which has 1 isolated observation in 1978 from Siding Spring Observatory. By performing the same analysis of Section 2.4 (see Fig. 3) we see no clear improvement due to Yarkovsky as the observation is 3.5–4σ away from the prediction either way. In this case a clock error may bring the Yarkovsky solution close to the observation. As this detection depends on a lone, isolated observation we would rather be cautious and consider this detection reliable only if the 1978 observation is remeasured.
- Eros, which looks like a reliable detection as $\mathscr{S} = 0.75$. However, the obliquity is known to be 89° (Yeomans et al., 2000) and then we enter the regime where the seasonal component of the Yarkovsky effect is dominant. As the seasonal component is typically 10 times smaller then the diurnal one (Vokrouhlický et al., 2000) we mark this detection as spurious. This points to possible bad astrometric treatment, especially for historical observations dating back to 1893.
- Toutatis, which enters the Main Belt region because of the 4.12 au aphelion and the low inclination (0.44°). Therefore, it is important to account for the uncertainty in the masses of the perturbing asteroids. By taking into account the uncertainty

Table 4
Same as Table 2 for small orbital drifts. Icarus' obliquity is from De Angelis (1995). All the other physical quantities are from the EARN database.

Asteroid	a (au)	e	H	D (km)	P (h)	A	γ	A_2 (10^{-15} au/d^2)	SNR	$\mathscr{S}$	da/dt (10^{-4} au/Myr)	da/dt Nugent et al.	Diff. σ	Observed arc	Radar apparitions
(1566) Icarus	1.08	0.83	16.7	1.30	2.27	0.04	103°	−0.66 ± 1.39	0.5	0.04	−0.86 ± 1.80	−3.2 ± 2.0	0.9	1949–2012	1968, 1996
(3757) 1982 XB	1.84	0.45	19.1	0.39	9.00	NA	NA	−17.06 ± 13.25	1.3	0.30	−6.68 ± 5.19	−13.7 ± 6.8	0.8	1982–2012	1987
(6239) Minos	1.15	0.41	18.3	0.47	3.56	0.26	NA	−9.34 ± 9.59	1.0	0.20	−4.45 ± 4.57	NA	NA	1983–2010	2004
(99907) 1989 VA	0.73	0.59	17.8	0.55	2.51	0.11	NA	8.71 ± 5.40	1.6	0.21	6.70 ± 4.15	NA	NA	1989–2012	NA
(161989) Cacus	1.12	0.21	17.1	0.6	3.75	NA	NA	7.97 ± 5.48	1.5	0.21	3.35 ± 2.30	2.6 ± 2.3	0.2	1978–2010	NA
(306383) 1993 VD	0.88	0.55	21.6	NA	NA	NA	NA	−16.01 ± 11.58	1.4	0.11	−10.43 ± 7.55	NA	NA	1993–2011	NA
2003 XV	1.92	0.55	26.6	NA	NA	NA	NA	−187.40 ± 272.02	0.7	0.14	−82.37 ± 119.56	NA	NA	2003–2011	NA
2004 FG_{11}	1.59	0.72	20.9	0.15	20.0	NA	NA	−29.98 ± 30.16	1.0	0.20	−21.24 ± 21.36	NA	NA	2004–2012	2012
2004 SC_{56}	0.77	0.43	22.8	NA	NA	NA	NA	−61.54 ± 51.38	1.2	0.26	−36.56 ± 30.52	NA	NA	2004–2010	NA
2005 ST_1	1.45	0.37	20.3	NA	NA	NA	NA	−12.31 ± 19.82	0.6	0.16	−5.03 ± 8.10	NA	NA	1991–2012	NA

of the perturbing asteroid masses the actual uncertainty in A_2 increases by 11% with a commensurable drop in SNR. Fig. 4 shows the evolution of A_2 as a function of the number of perturbers for asteroids 1999 RQ_{36} and Toutatis. While for 1999 RQ_{36} (aphelion 1.36 au) we reach convergence with just four perturbers, for Toutatis we have a quite irregular behavior suggesting that we may need to include more perturbers.

- 1994 XL_1, whose observations in 1994 from Siding Spring Observatory show high residual so we relaxed weights at 3″.
- 2005 QC_5 and 2000 NL_{10} have been included despite the low SNR. Similarly to the cases described in Section 2.4, we applied weights at 3″ to precovery observations and this data treatment weakened the Yarkovsky detection. However, we think that remeasuring the precovery observations may lead to reliable Yarkovsky detections for these objects.
- 1950 DA, for which the Yarkovsky effect plays an important role for impact predictions, e.g., see Section 4.4.

There are other objects with an even lower SNR for which the Yarkovsky signal might be revealed if precovery observations were remeasured: (11284) Belenus, (66400) 1999 LT_7, (4688) 1980 WF, (67399) 2000 PJ_6, (267759) 2003 MC_7, and (88710) 2001 SL_9.

Though these detections have to be considered less reliable, some of them may be good candidates for becoming stronger detections in the future if high quality astrometry is obtained, e.g., by radar or Gaia (Mignard, 2003).

The results presented so far do not capture those cases for which the orbital drift truly is small. In fact, when $da/dt \sim 0$ the SNR is unlikely to be greater than 1. Table 4 contains detections with SNR < 2 such that

$$\frac{|(A_2)_{exp}| - |A_2|}{\sigma_{A_2}} > 3 \tag{13}$$

This inequality ensures that the possible magnitude of the Yarkovsky effect is significantly smaller (3-σ level) than expected. In particular, for Icarus we obtain a strong constraint on A_2 and thus da/dt, which is consistent with Vokrouhlický et al. (2000, Fig. 5) where $|da/dt| < 3 \times 10^{-4}$ au/Myr. These cases are interesting as they might be an indication of obliquities near 90° (e.g., Icarus' obliquity is 103°), excessively slow rotations, high bulk density, or small thermal inertias.

4. Discussion

4.1. Connection with NEA feeding mechanisms

The diurnal Yarkovsky effect produces a semimajor axis drift proportional to $\cos\gamma$ (Vokrouhlický et al., 2000). As the diurnal term is typically the dominant one, the sign of da/dt can be related to the asteroid spin orientation, i.e., a negative da/dt corresponds to a retrograde rotator while a positive da/dt corresponds to a prograde rotator. This conclusion is supported by the eight known obliquities for the asteroids in the sample that are listed in Table 2: in all cases the spin axis obliquity is consistent with the sign of da/dt.

We can now use this interpretation and our solution for the Yarkovsky semimajor axis drift values for NEAs in the following way. Table 2 contains four prograde rotators and 17 retrograde rotators. This excess of retrograde rotators can be explained by the nature of resonance feeding into the inner Solar System (Bottke et al., 2002). Most of the primary NEA source regions (e.g., the 3:1 resonance, JFCs, Outer Belt, etc.) allow main belt asteroids to enter by drifting either inwards or outwards, but the ν_6 resonance is at the inner edge of the main belt and so asteroids can generally enter only by inwards drift, i.e., with retrograde rotation. Bottke et al. (2002) report that 37% of NEAs with absolute magnitude $H < 22$ arrive via ν_6 resonance. La Spina et al. (2004) point out that this implies 37% of NEAs have retrograde spin (via ν_6), plus half of the complement (via other pathways). Thus, the retrograde fraction should be $0.37 + 0.5 \times 0.63 = 0.69$, while La Spina et al. (2004) report 67% retrograde for their sample, which is dominated by large NEAs.

Table 2 contains 81% retrograde rotators, which is larger than 69% and thus, at face value, appears to be inconsistent with the theory. The sample of asteroids shown in Table 2, however, is based on measured Yarkovsky mobility and is not a representative sample of the debiased NEA population as described by Bottke et al. (2002). For example, the sample is dominated by small PHAs (MOID < 0.05 AU) on fairly deep Earth-crossing orbits. We find that 9 of the 21 objects are Aten asteroids (43%), compared to the 6% fraction predicted for the debiased NEA population. Bottke et al. (2002) suggest that the majority of Atens (∼79%) should come from the innermost region of the main belt where the ν_6 resonance is located. That would indicate the sampled objects are predisposed to have retrograde spin vectors.

To further quantify this, we used the debiased NEA model from Bottke et al. (2002) to determine the probability that the objects in Table 2 came from one of five intermediate source regions: the ν_6 secular resonance, the intermediate source Mars-crossing region (MC), the 3:1 mean motion resonance with Jupiter, the outer main belt (OB), and the transneptunian disk (which provides active and inactive Jupiter-family comets, JFCs). Our results are shown in Table 5. Next, we multiplied these values by a second set of probabilities corresponding to whether a given intermediate source would produce NEAs with prograde or retrograde spin vectors. Here we assumed the ν_6 resonance would only produce NEAs with retrograde spin vectors, while the other sources would provide a 50–50 mix of objects with prograde and retrograde spin vectors. Adding these probabilities together and normalizing by the number of objects in our sample, we predict that 79.3% of the objects in Table 2 should have retrograde spins. We therefore find an excellent match to the 81% ± 8% value provided by observations.

Asteroid 1999 MN represents a mismatch to the assumption that the ν_6 resonance produces NEAs with only retrograde spin. However, 1999 MN has a very peculiar orbit as it might have been evolving in the planet-crossing space for more than 50 Myr. During

Table 5
Probability of coming from one of the intermediate NEA source regions for the objects of Table 2.

Asteroid	ν_6 (%)	MC (%)	3:1 (%)	OB (%)	JFC (%)
1999 RQ_{36}	81.5	18.5	0.0	0.0	0.0
1992 BF	70.2	27.5	2.3	0.0	0.0
Golevka	15.9	21.7	39.6	22.8	0.0
2009 BD	78.8	21.2	0.0	0.0	0.0
Apollo	60.3	21.1	18.6	0.0	0.0
Aten	68.6	28.8	2.7	0.0	0.0
Nyx	65.0	20.2	5.3	9.5	0.0
Ra-Shalom	29.2	7.0	63.8	0.0	0.0
1989 ML	5.7	94.3	0.0	0.0	0.0
1999 MN	100.0	0.0	0.0	0.0	0.0
Hathor	75.2	19.2	5.6	0.0	0.0
1988 EG	60.2	26.7	13.1	0.0	0.0
Illapa	45.6	24.3	30.1	0.0	0.0
1999 FK_{21}	72.1	27.9	0.0	0.0	0.0
Toro	62.9	27.7	9.4	0.0	0.0
2005 ES_{70}	63.3	10.8	25.9	0.0	0.0
YORP	72.0	24.4	3.6	0.0	0.0
2001 MQ_3	17.9	73.9	5.2	3.0	0.0
Geographos	60.4	27.8	11.7	0.0	0.0
1989 UQ	64.2	15.0	20.8	0.0	0.0
1991 VE	63.8	1.3	34.9	0.0	0.0
Average	58.7	25.7	13.9	1.7	0.0

this time various things might have occurred, including a situation where the spin went over the end of a YORP cycle. Moreover, this body is a prime candidate for being affected by tidal forces during a close planetary encounter (i.e., high eccentricity Aten with low inclination). As a matter of fact, Hicks et al. (2010) already suggested the possibility of YORP and/or tidal spin-up. From its orbit, 1999 MN has a very high probability of encountering both Earth and Venus.

To assess the behavior of the fraction of retrograde rotators as a function of the SNR, we took all of the objects with $S < 1.5$. The left panel of Fig. 5 shows the distribution of A_2 and its uncertainty. The excess of retrograde rotators is clearly visible for SNR > 3 and also between 2 and 3, where small PHAs dominate. For lower SNR we have a more uniform distribution. The right panel of Fig. 5 is a running mean of the fraction of retrograde rotators as a function of the SNR. For SNR < 1 (372 objects) we are in a noise dominated regime for which we have a rough 50% fraction of retrograde rotators, for 1 < SNR < 2 (51 objects) we have a transition from noise-dominated to signal dominated, and for SNR > 2 (43 objects) we have a signal dominated regime with around 80% retrograde rotators.

We can also try to use the detected values to infer the obliquity distribution. From Eq. (10) we have that

$$A_2 \propto \frac{\cos\gamma}{D} \tag{14}$$

and so we can estimate γ by using the either known or estimated by Eq. (12) diameter and using 1999 RQ_{36}. By taking both the detections with SNR > 1 and those satisfying Eq. (13) with 1 as right hand side, and assuming a fixed $\rho = 1500\ \mathrm{kg/m^3}$ we obtain the distribution of Fig. 6, where the cases with $|\cos\gamma| > 1$ have been placed in the extreme obliquity bins. For the detections with SNR < 1 the nominal value of A_2 is not very reliable, so we added a random component corresponding to σ_{A_2}. Despite the low number of bins, we can see the excess of retrograde rotators and the abundance of objects with an extreme obliquity, as expected from the YORP effect (Čapek and Vokrouhlický, 2004). While this distribution should be considered only approximate due to the numerous assumptions (e.g., neglecting dependence on bulk density, shape and thermal properties) we consider it to be a significant improvement over what is otherwise known. However, we find it interesting that it appears to be consistent with the observed obliquity distribution of the NEAs (La Spina et al., 2004).

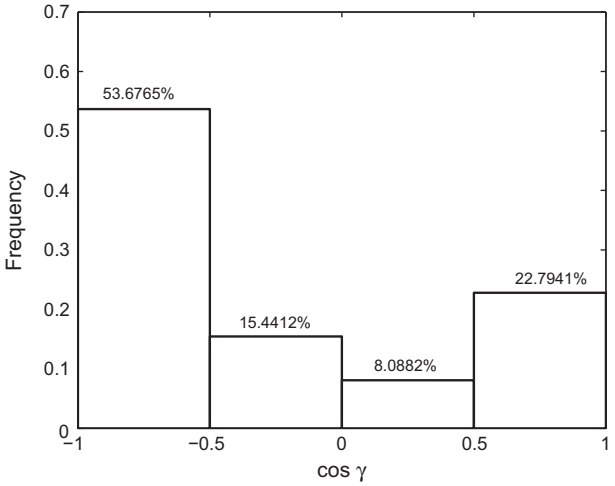

Fig. 6. Inferred obliquity distribution based on 136 objects.

4.2. Spurious detections

Our search for Yarkovsky signal produced a large number of spurious detections, i.e., semimajor axis drifts far larger than the Yarkovsky effect would cause. Fig. 7 contains the histograms of $\mathscr{S}$ for different SNR intervals. For SNR > 3 we have 67% spurious detections, for 2 < SNR < 3 we have 88%.

It is worth trying to understand the reason of these spurious solutions. We think there are two possible causes:

- Bad astrometry treatment: as discussed in Sections 2.3 and 2.4, non-CCD observations may contain errors that are difficult to model. If an ad hoc weighting is not used we may have misleading results. Indeed, spot checking of such cases generally confirmed isolated astrometry as source of spurious detections.
- Incompleteness or inconsistency in the dynamical model: the formulation proposed in Section 2.1 is a simplified model of the Yarkovsky perturbation that might be poor in some cases. A more sophisticated formulation would require a rather complete physical characterization that is typically unavailable and thus cannot be used for a comprehensive search as done in this paper. Moreover, as discussed in Section 3.3 for Toutatis,

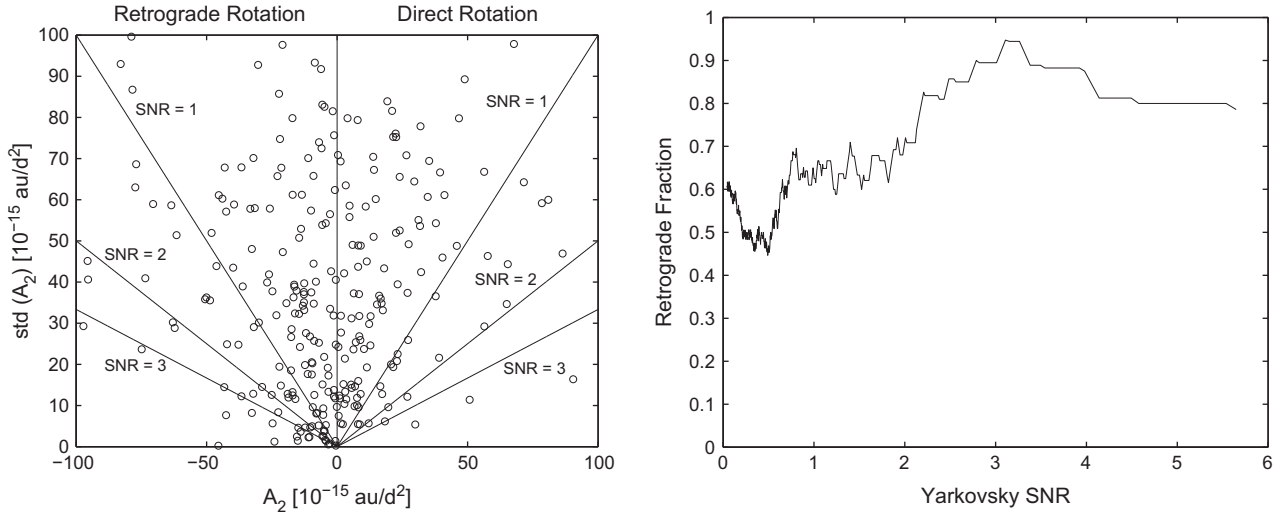

Fig. 5. Left panel: distribution of A_2 and its uncertainty. Right side of plot is prograde rotation and left side is retrograde rotation. Right panel: running box mean in SNR for the fraction of asteroids with indication of retrograde spin. Cases with SNR > 2 show a consistent 4:1 retrograde ratio, cases with little or no signal are split 50–50.

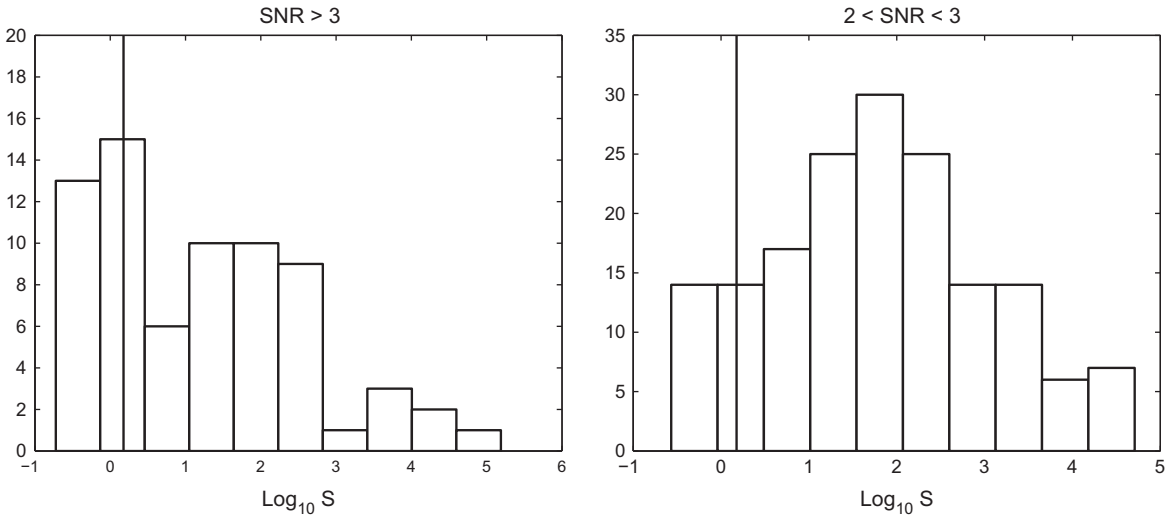

Fig. 7. Histogram of $\mathscr{S}$ for different intervals of SNR. The vertical lines correspond to the selected threshold 1.5.

we may need to include more perturbing asteroids (and the uncertainty in their masses) in the model. Finally, we cannot rule out the possibility of nongravitational perturbations different from Yarkovsky as also discussed by Nugent et al. (2012b).

4.3. Constraining physical quantities

The results reported in Table 2 can be used to constrain physical quantities. When A, D, and γ are known Eq. (10) provides a simple relationship between ρ and Θ. This relationship can be easily translated into a relationship between ρ and the thermal inertia Γ by means of Eq. (9). As a benchmark of this technique we can use asteroid 1999 RQ_{36} (Fig. 8), for which the known values of Γ and ρ (Chesley et al., 2012) match the plotted constraint. Fig. 9 shows the possible values of ρ as a function of Γ for asteroids Golevka, Apollo, Ra-Shalom, Toro, YORP, and Geographos. For the last two objects we assumed slope parameter $G = 0.15$. Our findings are consistent with the taxonomic type. For instance, Golevka, Apollo, Toro, YORP, and Geographos are S/Q-type asteroids with an expected density between 2000 and 3000 kg/m^3, while Ra-Shalom is a C-type so we expect a bulk density from 500 and 1500 kg/m^3. Fig. 9 suggests that Golevka has thermal inertia $150 < \Gamma < 500$ J m^{-2} s$^{-0.5}$ K^{-1} zand Apollo has a rather large thermal inertia $400 < \Gamma < 1000$ J m^{-2} - s$^{-0.5}$ K^{-1}. According to Delbó et al. (2003) Ra-Shalom has an unusually high thermal inertia. In fact, by taking the right side of the plotted rectangle we obtain a density closer to 1000 kg/m^3, similar to the one 1999 RQ_{36}, which belongs to a similar taxonomic class. For Toro, Mueller (2012) reports a thermal inertia $200 < \Gamma < 1200$ J m^{-2} s$^{-0.5}$ K^{-1} but likely lower, which would result in a bulk density between 2000 and 4000 kg/m^3.

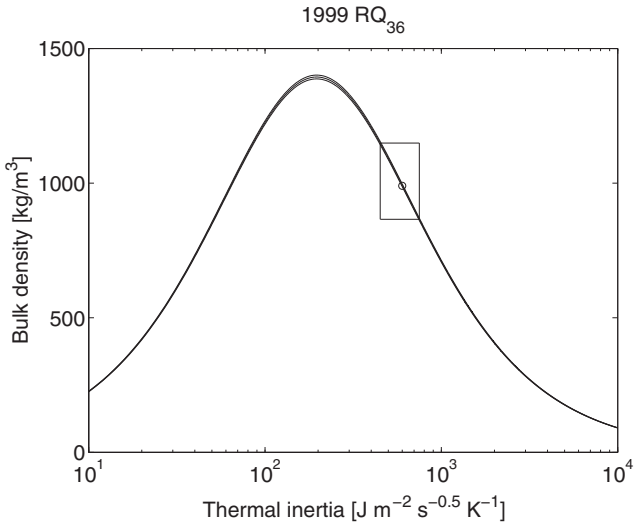

Fig. 8. Density as a function of thermal inertia for asteroid 1999 RQ_{36}. The three lines corresponding to the nominal value and the 1-σ levels are extremely narrow because of the high SNR. The circle corresponding to the nominal observed value of Γ and thus inferred nominal value of ρ (Chesley et al., 2012) matches the plotted curves. The enclosed region corresponds to the 1-σ interval for Γ (Emery et al., 2012) and indicates how it maps onto the 1-σ limits of ρ.

4.4. Implications for impact predictions

There are three known asteroids, namely Apophis, 1999 RQ_{36}, and 1950 DA, for which Yarkovsky perturbations are relevant and need to be accounted for in the impact risk assessment. For Apophis and 1999 RQ_{36} this is due to the presence of a strongly scattering planetary close approach between now and the epochs of the possible impacts. These encounters transform a very well determined orbit into a poorly known one for which chaotic effects are dominant (Milani et al., 2009). Apophis will have a close approach in April 2029 with minimum distance of ~38,000 km from the geocenter. As a consequence the orbital uncertainty will increase by a factor >40,000. 1999 RQ_{36} will have a close approach to Earth in 2135 with nominal minimum distance about the same as the distance to the Moon, with an increase in uncertainty by a factor ~500. The minimum possible distance for this close approach is three times smaller and would result in an increase of the uncertainty by a factor ~1500 (Chesley et al., 2012). In both cases the Yarkovsky effect is large enough to shift the position at the scattering close approach by an amount much larger than the distance between the keyholes (Chodas, 1999) corresponding to impacts in later years (2036, 2037, 2068 for Apophis; 2175, 2180, 2196 for 1999 RQ_{36}). Thus, the occurrence of these later impacts is determined by the Yarkovsky perturbation in the years between now and the scattering encounter. For 1950 DA the influence of the Yarkovsky effect for the possible impact in 2880 is due to the long time interval preceding the impact that allows the orbital displacement to accumulate (Giorgini et al., 2002).

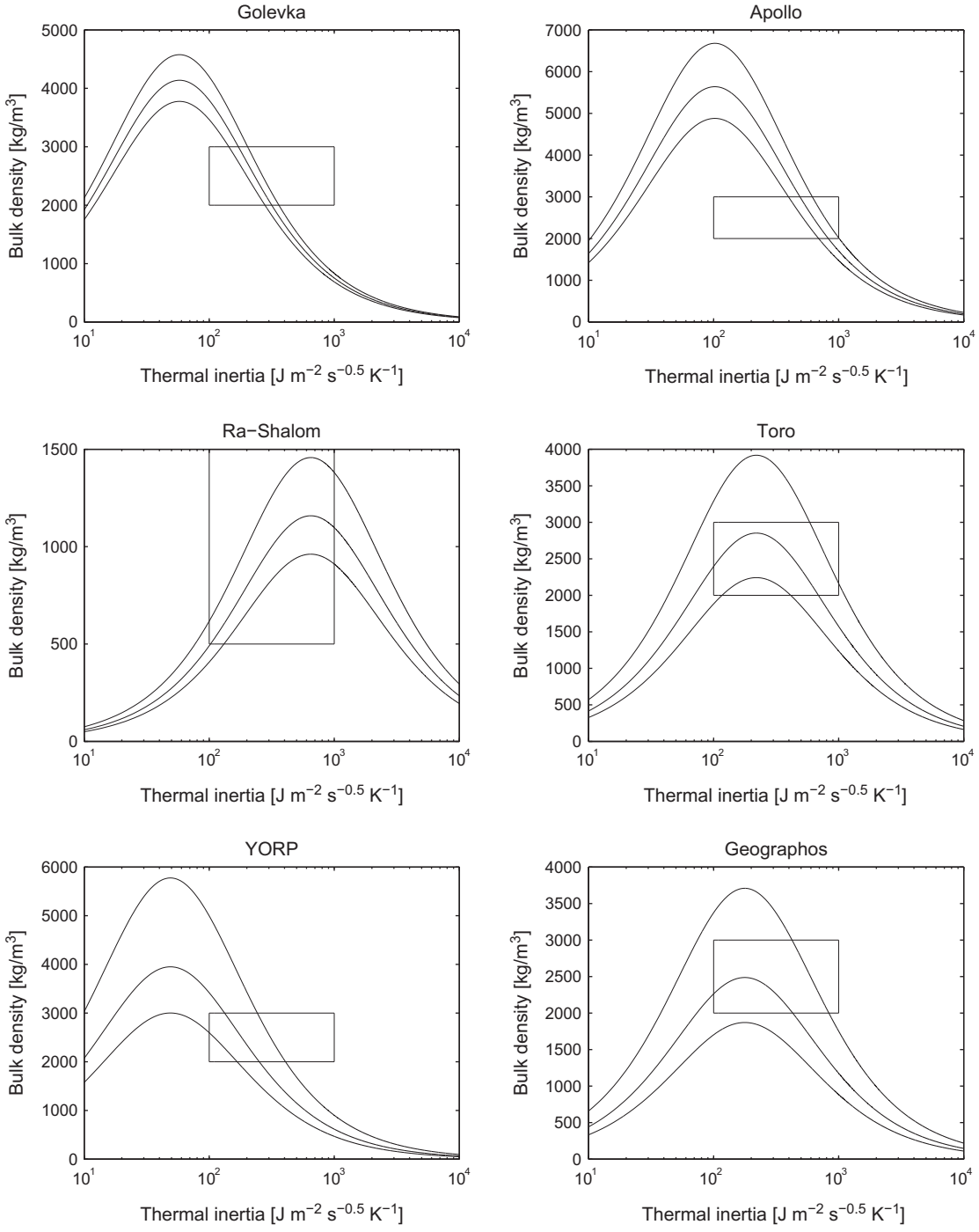

Fig. 9. Density as a function of thermal inertia for asteroids Golevka, Apollo, Ra-Shalom, Toro, YORP, and Geographos. The rectangles correspond to reasonable values of ρ according to the taxonomic type and to a reasonable range of Γ (Delbó et al., 2007).

Currently, 1999 RQ_{36} is the case with the best determined Yarkovsky effect (SNR $\sim$ 200), while Apophis and 1950 DA have only a marginal detection (SNR < 1 and SNR $\sim$ 1.4, respectively). Therefore, the impact monitoring for 1999 RQ_{36} fully takes into account the Yarkovsky effect (Chesley et al., 2012). On the contrary, the current estimate of impact probabilities for Apophis is based on a Monte Carlo model of the Yarkovsky perturbation based on a priori knowledge of the statistical properties of this effect (Chesley et al., 2009). 1950 DA could benefit from a similar approach.

We investigated the possibility that our identification of asteroids with measurable Yarkovsky effect produces new cases such as the two above, that is of impact monitoring affected by the Yarkovsky perturbation. The answer to this question is negative, in that the intersection between the current list of NEAs with possible impacts on Earth (404 according to Sentry, 337 according to NEODyS) and the list with detected Yarkovsky orbital drifts contains only 1999 RQ_{36}.

However, this conclusion depends on the fact that our monitoring of possible future impacts is done for only about one century (currently 100 for Sentry, 90 years for NEODyS). 1999 RQ_{36} was a special case, related to an intensified effort for the OSIRIS-REx mission target (http://osiris-rex.lpl.arizona.edu). If this time span were generally increased to 150–200 years, there could well be other cases similar to 1999 RQ_{36}.

For asteroid 1950 DA Busch et al. (2007) report a minimum density around 3000 kg/m^3 and two possible solutions for pole orientation and effective diameter:

1. $\gamma = 24.47^\circ$ and $D = 1.16$ km;
2. $\gamma = 167.72^\circ$ and $D = 1.30$ km.

By scaling from the 1999 RQ_{36} case, we obtain $A_2 = 7.01 \times 10^{-15}$ au/d^2 for the direct solution and $A_2 = -5.83 \times 10^{-15}$ au/d^2 for the retrograde solution. Even if we found a low SNR detection, our result strongly favors the retrograde solution, which is at 0.6σ, than the direct solution, which is more than 3σ away. According to Giorgini et al. (2002), the 2880 impact is ruled out by retrograde rotation.

5. Conclusions

High precision orbit estimation for asteroids is important in several applications such as linking old observations to a newly discovered object and assessing the risk of an Earth impact. In these cases, the Yarkovsky perturbation is a critical component as it is usually unknown. We measured reliable orbital drifts for 21 objects and we expect to have more as new high precision data, e.g., radar and Gaia observations, are available. Inaccurate astrometric treatments can lead to unrealistic results, especially when the Yarkovsky drift significantly depends on isolated observations. When a rather complete physical model is available, the measured orbital drifts can be used to measure unknown physical quantities such as the bulk density. The distribution of the detected orbital drifts can be connected to the NEA delivery mechanism and serve as a validation of future NEA models. For asteroids experiencing deep close approaches, the occurrence of an impact can be decisively driven by the magnitude of the Yarkovsky perturbation.

6. Note added in proof

We have identified an additional high SNR detection, namely 2002 XQ_{40}, with $A_2 = -94.23 \pm 6.12$ and da/dt = 44.03 ± 2.86. This corresponds to SNR $\sim$15, which should be solidified by remeasurement of isolated observations in 1954. As the asteroid observational database continues to grow and be refined we intend to maintain a updated list of Yarkovsky detections at URL ftp://ssd.jpl.nasa.gov/pub/ssd/yarkovsky/.

Acknowledgments

D.F. was supported for this research in part by an appointment to the NASA Postdoctoral Program at the Jet Propulsion Laboratory, California Institute of Technology, administered by Oak Ridge Associated Universities through a contract with NASA, and in part by ESA/ESTEC-SpaceDyS Service Level Agreement SSA-NEO-ESA-SLA2-002_NEODYS.

S.C. conducted this research at the Jet Propulsion Laboratory, California Institute of Technology, under a contract with the National Aeronautics and Space Administration.

The work of D.V. was partially supported by the Czech Grant Agency (Grant 205/08/0064) and Research Program MSM002162 0860 of the Czech Ministry of Education.

References

Baer, J., Chesley, S.R., Matson, R.D., 2011. Astrometric masses of 26 asteroids and observations on asteroid porosity. Astron. J. 141, 143–154.

Bottke, W.F., Morbidelli, A., Jedicke, R., Petit, J.-M., Levison, H.F., Michel, P., Metcalfe, T.S., 2002. Debiased orbital and absolute magnitude distribution of the Near-Earth Objects. Icarus 156, 399–433.

Bottke Jr., W.F., Vokrouhlický, D., Rubincam, D.P., Nesvorný, D., 2006. The Yarkovsky and Yorp effects: Implications for asteroid dynamics. Annu. Rev. Earth Planet. Sci. 34, 157–191.

Bowell, E., Hapke, B., Domingue, D., Lumme, K., Peltoniemi, J., Harris, A.W., 1989. Application of photometric models to asteroids. In: Binzel, R.P., Gehrels, T., Matthews, M.S. (Eds.), Asteroids II. Tucson, AZ, University of Arizona Press, pp. 524–556.

Brozović, M., Ostro, S.J., Benner, L.A.M., Giorgini, J.D., Jurgens, R.F., Rose, R., Nolan, M.C., Hine, A.A., Magri, C., Scheeres, D.J., Margot, J.-L., 2009. Radar observations and a physical model of Asteroid 4660 Nereus, a prime space mission target. Icarus 201, 153–166.

Busch, M.W., Giorgini, J.D., Ostro, S.J., Benner, L.A.M., Jurgens, R.F., Rose, R., Hicks, M.D., Pravec, P., Kusnirak, P., Ireland, M.J., Scheeres, D.J., Broschart, S.B., Magri, C., Nolan, M.C., Hine, A.A., Margot, J.-L., 2007. Physical modeling of Near-Earth Asteroid (29075) 1950 DA. Icarus 190, 608–621.

Čapek, D., Vokrouhlický, D., 2004. The YORP effect with finite thermal conductivity. Icarus 172, 526–536.

Carpino, M., Milani, A., Chesley, S.R., 2003. Error statistics of asteroid optical astrometric observations. Icarus 166, 248–270.

Chesley, S.R., Chodas, P.W., Milani, A., Valsecchi, G.B., Yeomans, D.K., 2002. Quantifying the Risk Posed by Potential Earth Impacts. Icarus 159, 423–432.

Chesley, S.R. et al., 2003. Direct detection of the Yarkovsky effect by radar ranging to Asteroid 6489 Golevka. Science 302, 1739–1742.

Chesley, S.R. et al., 2008. Direct estimation of Yarkovsky accelerations on Near-Earth Asteroids. LPI Contrib. 1405, 8330.

Chesley, S.R., Milani, A., Tholen, D., Bernardi, F., Chodas, P., Micheli, M., 2009. An updated assessment of the impact threat from 99942 Apophis. In: AAS/Division for Planetary Sciences Meeting Abstracts #41, vol. 41, p. #43.06 (abstract).

Chesley, S.R., Baer, J., Monet, D.G., 2010. Treatment of star catalog biases in asteroid astrometric observations. Icarus 210, 158–181.

Chesley, S.R. et al., 2012. The trajectory dynamics of Near-Earth Asteroid 101955 (1999 RQ36).Asteroids, Comets, Meteors 2012, Proceedings of the conference held May 16-20, 2012 in Niigata, Japan. LPI Contribution No. 1667, id.6470.

Chodas, P.W., 1999. Orbit uncertainties, keyholes, and collision probabilities. In: Bulletin of the American Astronomical Society, vol. 31, p. 1117.

De Angelis, G., 1995. Asteroid spin, pole and shape determinations. Planet. Space Sci. 43, 649–682.

Delbó, M., Harris, A.W., Binzel, R.P., Pravec, P., Davies, J.K., 2003. Keck observations of Near-Earth Asteroids in the thermal infrared. Icarus 166, 116–130.

Delbó, M., Dell'Oro, A., Harris, A.W., Mottola, S., Mueller, M., 2007. Thermal inertia of Near-Earth Asteroids and implications for the magnitude of the Yarkovsky effect. Icarus 190, 236–249.

Drummond, J.D., Wisniewski, W.Z., 1990. The rotational poles and shapes of 1580 Betulia and 3908 (1980PA) from one apparition. Icarus 83, 349–359.

Ďurech, J. et al., 2008a. Detection of the YORP effect in Asteroid (1620) Geographos. Astron. Astrophys. 489, L25–L28.

Ďurech, J. et al., 2008b. New photometric observations of Asteroids (1862) Apollo and (25143) Itokawa – An analysis of YORP effect. Astron. Astrophys. 488, 345–350.

Ďurech, J. et al., 2012. Analysis of the rotation period of Asteroids (1865) Cerberus, (2100) Ra-Shalom, and (3103) Eger – Search for the YORP effect. Astron. Astrophys. 547, A10–A18.

Emery, J.P. et al., 2012. Thermal and physical characterization of the OSIRIS-REx target Asteroid (101955) 1999 RQ36. In: AAS/Division for Planetary Sciences Meeting Abstracts, vol. 44. p. #102.05 (abstract).

Giorgini, J.D. et al., 2002. Asteroid 1950 DA's encounter with Earth in 2880: Physical limits of collision probability prediction. Science 296, 132–136.

Giorgini, J.D., Benner, L.A.M., Ostro, S.J., Nolan, M.C., Busch, M.W., 2008. Predicting the Earth encounters of (99942) Apophis. Icarus 193, 1–19.

Hicks, M., Mayes, D., McAuley, A., Foster, J., 2010. Broadband photometry of the potentially hazardous Asteroid 1999 MN: Suggestive of YORP and/or tidal spin-up? Astronomer's Telegram #2706.

Hudson, R.S., Ostro, S.J., Jurgens, R.F., Rosema, K.D., Giorgini, J.D., Winkler, R., Rose, R., Choate, D., Cormier, R.A., Franck, C.R., Frye, R., Howard, D., Kelley, D., Littlefair, R., Slade, M.A., Benner, L.A.M., Thomas, M.L., Mitchell, D.L., Chodas, P.W., Yeomans, D.K., Scheeres, D.J., Palmer, P., Zaitsev, A., Koyama, Y., Nakamura, A., Harris, A.W., Meshkov, M.N., 2000. Radar observations and physical model of Asteroid 6489 Golevka. Icarus 148, 37–51.

Konopliv, A.S., Asmar, S.W., Folkner, W.M., Karatekin, Ö., Nunes, D.C., Smrekar, S.E., Yoder, C.F., Zuber, M.T., 2011. Mars high resolution gravity fields from MRO, Mars seasonal gravity, and other dynamical parameters. Icarus 211, 401–428.

La Spina, A., Paolicchi, P., Kryszczyńska, A., Pravec, P., 2004. Retrograde spins of Near-Earth Asteroids from the Yarkovsky effect. Nature 428, 400–401.

Marsden, B.G., Sekanina, Z., Yeomans, D.K., 1973. Comets and nongravitational forces. V. Astron. J. 78, 211–225.

Micheli, M., Tholen, D.J., Elliott, G.T., 2012. Detection of radiation pressure acting on 2009 BD. New Astron. 17, 446–452.

Mignard, F., 2003. Observations of small Solar System bodies with GAIA. In: IAU Joint Discussion, vol. 19, p. 737.

Milani, A., Chesley, S.R., Sansaturio, M.E., Bernardi, F., Valsecchi, G.B., Arratia, O., 2009. Long term impact risk for (101955) 1999 RQ. Icarus 203, 460–471.

Moyer, T.D., 2003. Formulation for Observed and Computed Values of Deep Space Network Data Types for Navigation. Wiley-Interscience, Hoboken, NJ.

Mueller, M., 2012. Surface Properties of Asteroids from Mid-Infrared Observations and Thermophysical Modeling. ArXiv e-prints.

Nugent, C.R., Mainzer, A., Masiero, J., Grav, T., Bauer, J., 2012a. The Yarkovsky drift's influence on NEAs: Trends and predictions with NEOWISE measurements. Astron. J. 144, 75–80.

Nugent, C.R., Margot, J.L., Chesley, S.R., Vokrouhlický, D., 2012b. Detection of semimajor axis drifts in 54 Near-Earth Asteroids: New measurements of the Yarkovsky effect. Astron. J. 144, 60–72.

Pravec, P., Harris, A.W., 2007. Binary asteroid population. 1. Angular momentum content. Icarus 190, 250–259.

Rozitis, B., Green, S.F., 2012. The influence of rough surface thermal-infrared beaming on the Yarkovsky and YORP effects. Mon. Not. R. Astron. Soc. 423, 367–388.

Standish, E.M., 2000. Recommendation of DE405 for 2001 Mars Surveyor and for Cassini. Tech. Rep. IOM 312.F-00-107b, Jet Propulsion Laboratory.

Standish, E.M., Hellings, R.W., 1989. A determination of the masses of Ceres, Pallas, and Vesta from their perturbations upon the orbit of Mars. Icarus 80, 326–333.

Taylor, P.A. et al., 2007. Spin rate of Asteroid (54509) 2000 PH5 increasing due to the YORP effect. Science 316, 274–277.

Vokrouhlický, D., 1998. Diurnal Yarkovsky effect as a source of mobility of meter-sized asteroidal fragments. I. Linear theory. Astron. Astrophys. 335, 1093–1100.

Vokrouhlický, D., 1999. A complete linear model for the Yarkovsky thermal force on spherical asteroid fragments. Astron. Astrophys. 344, 362–366.

Vokrouhlický, D., Milani, A., Chesley, S.R., 2000. Yarkovsky effect on small Near-Earth Asteroids: Mathematical formulation and examples. Icarus 148, 118–138.

Vokrouhlický, D., Chesley, S.R., Matson, R.D., 2008. Orbital identification for Asteroid 152563 (1992 Bf) through the Yarkovsky effect. Astron. J. 135, 2336–2340.

Will, C.M., 1993. Theory and Experiment in Gravitational Physics. Cambridge University Press.

Yeomans, D.K. et al., 2000. Radio science results during the NEAR-Shoemaker spacecraft rendezvous with Eros. Science 289, 2085–2088.